JOURNAL OF MATERIALS SCIENCE 20 (1985) 2417–2438

Two-stage enthalpy relaxation behaviour of $(Fe_{0.5}Ni_{0.5})_{83}P_{17}$ and $(Fe_{0.5}Ni_{0.5})_{83}B_{17}$ amorphous alloys upon annealing

H. S. CHEN
AT and T Bell Laboratories, Murray Hill, New Jersey 07974, USA

A. INOUE, T. MASUMOTO
The Research Institute for Iron, Steel and Other Metals, Tohoku University, Sendai 980, Japan

The anneal-induced enthalpy relaxation behaviour for $(Fe_{0.5}Ni_{0.5})_{83}P_{17}$ and $(Fe_{0.5}Ni_{0.5})_{83}B_{17}$ amorphous alloys was examined calorimetrically. Upon heating the sample annealed at temperatures below T_g, an excess endothermic reaction (enthalpy relaxation) occurs above T_a. The $\Delta C_{p,endo}$ evolves reversibly in a continuous manner with $\ln t_a$. The changes in the magnitude of $\Delta C_{p,endo}$ and ΔH_{endo} with T_a show clearly two distinct stages; a low-temperature one which peaks at about $T_g - 200$ K and a high-temperature peak just below T_g. The activation energy, Q_m, increases with the peak temperature of ΔC_p, T_m, from 1.7 to 2.5 eV for the Fe–Ni–P and from 1.8 to 2.0 eV for the Fe–Ni–B for the low-temperature peak, and from 2.6 to 5.0 eV for the Fe–Ni–P for the high-temperature peak. The reversible change in T_c for the Fe–Ni–P alloy pre-annealed for 1 min at 640 K as a function of T_a was also found to show two stages; a low-temperature stage ranging from 400 to 550 K where T_c rises, and a high-temperature one above 550 K where T_c lowers. From the almost complete agreement of the temperature region and the peak temperature for each stage as well as the marked contrast in the change of T_c, it was proposed that the low-temperature endothermic peak is attributed to local and medium range rearrangements of metallic (iron and nickel) atoms and the high-temperature reaction to the long-range cooperative regroupings of metallic and metalloid atoms. The mechanism for the appearance of the two-stage enthalpy relaxation was investigated based on the new concept of two-stage distribution in relaxation times (or glass transitions) centring at T_{g1} and T_{g2} which arise respectively from the metal atoms and from the metal–metalloid atoms and the distinct two-stage splitting was interpreted to generate by the distinctly distinguishable difference in the easiness of structural relaxation between metal–metal and metal–metalloid. It was further found that the present irreversible and reversible enthalpy relaxation results are fairly well interpreted by a possible mechanism of two-stage relaxation processes consisting of as-quenched amorphous → local and medium range relaxation of metal atoms → cooperative relaxation of metal and metalloid atoms.

1. Introduction

Iron-based amorphous alloys were recently found to possess a number of practically useful characteristics such as high strength, good soft ferromagnetic properties, invar and elinvar effects, large magnetostriction, ΔE effect and so forth (e.g. [1]), and hence attract the most intense interest among a large number of amorphous

0022–2461/85 $03.00 + .12

alloy systems. Usually, these materials are thermally relaxed at an elevated temperature with an aim to remove an internal stress and improve various kinds of characteristics. However, there is a serious disadvantage that all of the iron-based amorphous alloys become brittle by annealing even at temperatures well below T_g and/or T_x. From the above-described points of view, a large number of studies on the effect of annealing on the structural relaxation as well as mechanical and physical properties have been carried out. There remains, however, an important unresolved problem about the difference in the influence of phosphorus and boron elements, which are essential metalloid elements for the formation of iron–metalloid type amorphous alloys, on the structural relaxation behaviour. More recently, it has been found for the iron-based amorphous alloys such as Fe–Ni–P–B–(Al) [2–4] and (Fe, Co, Ni)–Si–B [5] systems that the amorphous alloys annealed at temperatures well below glass transition temperature (T_g) or crystallization temperature (T_x) exhibit a reversible endothermic peak at a temperature slightly higher than the annealing temperature (T_a) and the further heating results in the same irreversible exothermic reaction as that of the as-quenched sample. In particular, the reversible endothermic phenomenon as a function of T_a in (Fe, Co, Ni)$_{75}$Si$_{10}$B$_{15}$ alloys was found to occur at two stages. The two-stage relaxation phenomenon cannot be satisfactorily interpreted by the previous model [6] on the one-stage structural relaxation which was proposed based on the data of $Pd_{48}Ni_{32}P_{20}$ amorphous alloy. This paper intends (1) to clarify quantitatively the T_a and t_a dependences of the anneal-induced structural relaxation behaviour, especially the enthalpy relaxation behaviour, for amorphous $(Fe_{0.5}Ni_{0.5})_{83}P_{17}$ and $(Fe_{0.5}N_{0.5})_{83}B_{17}$ alloys, (2) to investigate the difference in the influence of phosphorus and boron on the enthalpy relaxation behaviour, (3) to obtain the further detailed information on the two-stage enthalpy relaxation which was previously found for the first time for (Fe, Co, Ni)–Si–B system [5], and (4) to propose a new mechanism on two-stage structural relaxation of an amorphous alloy.

2. Experimental methods

Amorphous ribbons $(Fe_{0.5}Ni_{0.5})_{83}P_{17}$ and $(Fe_{0.5}Ni_{0.5})_{83}B_{17}$ ternary alloys, typically 20 μm in thickness and 1.5 mm in width, were prepared by a single-roller melt spinning method and confirmed to be amorphous by conventional X-ray diffractometer using Cu$K\alpha$ radiation in combination with an X-ray monochromator. The subscripts are assumed to be those of the unalloyed pure elements since the difference between nominal and chemically analysed compositions was less than 0.18 wt % for phosphorus and 0.09 wt % for boron. The apparent specific heat, C_p, and the Curie temperature, T_c, were measured with a differential scanning calorimeter (Perkin-Elmer DSC-II). Care was taken to reduce the thermal drift by prewarming the calorimeter for at least 5 h in the temperature range of interest. The accuracy of the data was about 0.8 J mol^{-1} K^{-1} for the absolute C_p values, but was better than 0.4 J mol^{-1} K^{-1} for the relative C_p or ΔC_p measurement and 1 K for the T_c measurement.

The as-quenched samples were subjected to annealing treatments at various temperatures below T_g(T_a = 350 to 600 K) for different periods (t_a = 1 to 48 h). Short-period anneals ($t_a \leqslant 13$ h) were performed directly inside the calorimeter while long-duration anneals (14 to 48 h) were performed in a well-controlled furnace after placing the encapsulated samples inside a vacuum-sealed quartz tube.

Following the annealing treatment, the sample was thermally scanned at 40 K min^{-1} from 320 to 680 K to determine the $C_{p,a}$ of the annealed sample. It was then cooled to 320 K, and reheated immediately to obtain the $C_{p,s}$ data of the "reference" sample (i.e. the preconditioned sample without further low-temperature annealing). This test procedure is essential in order to eliminate any possible error that might result from the drift in the calorimeter due to the prolonged annealing time between the measurements. The change in the calorimeter behaviour with annealing was used to monitor the structural relaxation processes.

3. Results

3.1. $C_p(T)$ and $\Delta C_p(T)$ behaviour of as-quenched samples

Fig. 1 shows the thermograms of an amorphous $(Fe_{0.5}Ni_{0.5})_{83}P_{17}$ alloy in as-quenched state. The C_p value of the as-quenched phase is about 26.2 J mol^{-1} K^{-1} near room temperature. As the temperature rises, the C_p value begins to decrease indicative of a structural relaxation at about 375 K, exhibits two minimum peaks at about 480 K and about 600 K in the range below 650 K, then

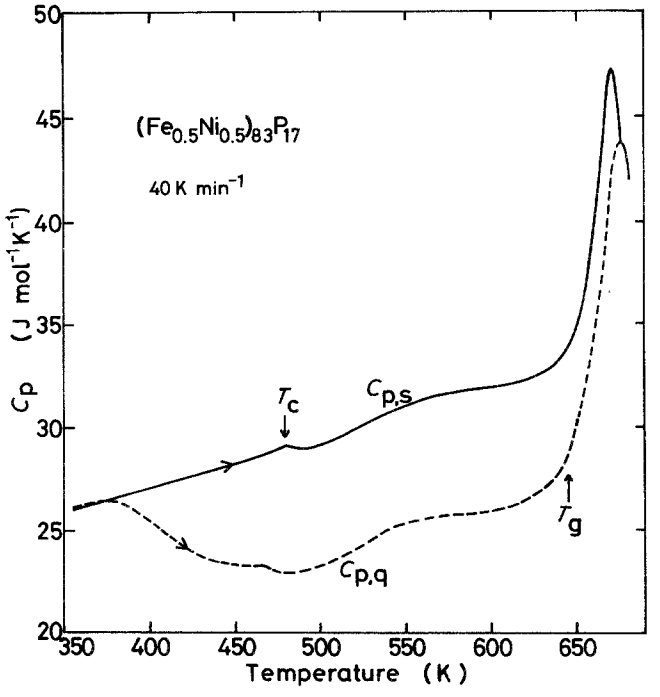

Figure 1 The thermogram of an amorphous $(Fe_{0.5}Ni_{0.5})_{83}P_{17}$ alloy in as-quenched state. The solid line presents the thermogram of the sample subjected to heating to 675 K.

increases rapidly in the region of glass transition and reaches an equilibrium liquid value of about 43.7 J mol^{-1} K^{-1} around 680 K. It can be seen that the C_p value near room temperature is consistently higher by about 0.1 to 0.2 J mol^{-1} K^{-1} for the as-quenched sample than for the annealed one. The small difference in C_p is attributed to the anneal-induced changes in physical and mechanical properties. The similar thermograms are obtained for an amorphous $(Fe_{0.5}Ni_{0.5})_{83}B_{17}$ alloy as shown in Fig. 2. However, it may be noted that (1) the temperature at which the exothermic reaction corresponding to an irreversible structural relaxation begins to occur is higher by about 30 K for the Fe–Ni–B alloy than for the Fe–Ni–P alloy, (2) no distinct glass transition phenomenon is recognized for the Fe–Ni–B alloy, (3) the splitting of the irreversible structural relaxation into two stages for the Fe–Ni–B alloy is not as clear as that for the Fe–Ni–P alloy, and (4) the Curie temperature of the Fe–Ni–P alloy is located in the vicinity of 475 K, whereas that of the

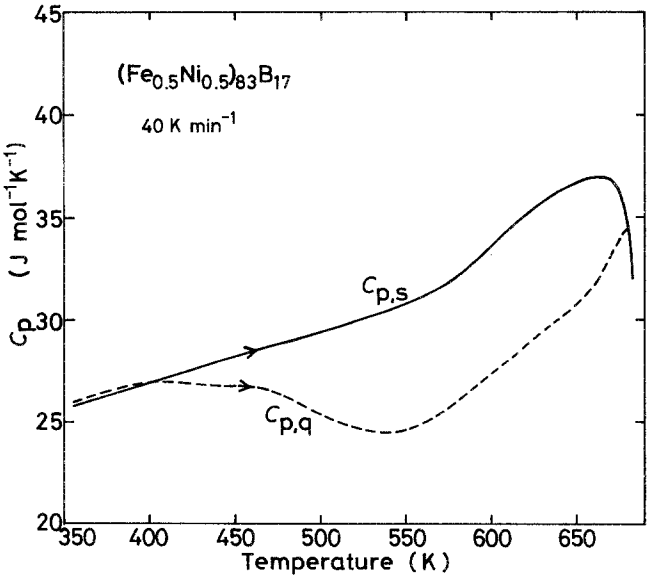

Figure 2 The thermogram of an amorphous $(Fe_{0.5}Ni_{0.5})_{83}B_{17}$ alloy in as-quenched state. The solid line presents the thermogram of the sample subjected to heating to 665 K.

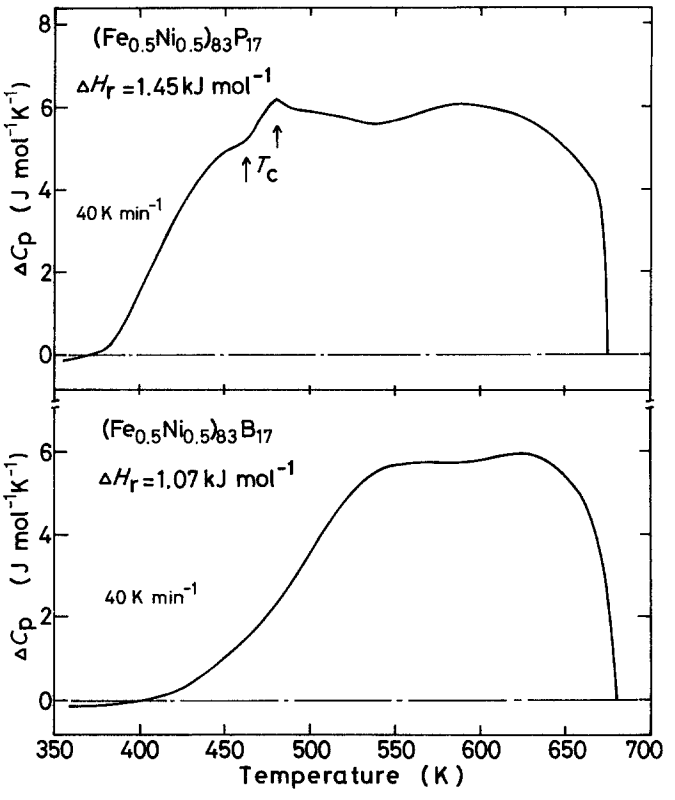

Figure 3 Difference in the specific heat between the as-quenched and annealed state ($\Delta C_{p,i,exo}$) plotted against temperature for amorphous $(Fe_{0.5}Ni_{0.5})_{83}P_{17}$ and $(Fe_{0.5}Ni_{0.5})_{83}B_{17}$ alloys.

Fe–Ni–B alloy is higher than the onset temperature of crystallization ($T_x \simeq 681$ K).

Fig. 3 shows the temperature dependence of the difference in C_p between the as-quenched and the annealed states $[\Delta C_p(T)]$ for the amorphous $(Fe_{0.5}Ni_{0.5})_{83}P_{17}$ and $(Fe_{0.5}Ni_{0.5})_{83}B_{17}$ alloys. Although the $\Delta C_p(T)$ curve of the Fe–Ni–P alloy is slightly complicated due to the appearance of Curie point, two separable broad irreversible relaxation peaks can be seen in the $\Delta C_p - T$ relation of the Fe–Ni–P and Fe–Ni–B alloys: a low-temperature one which peaks at about 480 K for $(Fe_{0.5}Ni_{0.5})_{83}P_{17}$ and about 540 K for $(Fe_{0.5}Ni_{0.5})_{83}B_{17}$ and a high-temperature peak at about 590 K for the former alloy and 625 K for the latter alloy. The appearance of two peaks in the $\Delta C_p - T$ relation for the as-quenched sample has been recognized for a number of amorphous alloys [7]. The value of $\Delta H_{i,exo}$ ($\equiv \int \Delta C_p dT$) for the Fe–Ni–P (1.45 kJ mol^{-1}) is larger by about 50% than that for the Fe–Ni–B (1.07 kJ mol^{-1}) due mainly to the incomplete relaxation of the latter, as the $\Delta C_{p,max}$ value is nearly equal ($\simeq 6$ J mol^{-1} K^{-1}) for both the alloys.

3.2. $C_p(T)$ and $\Delta C_p(T)$ behaviour of annealed samples

The changes in the thermograms of an amorphous $(Fe_{0.5}Ni_{0.5})_{83}P_{17}$ alloy with annealing temperature T_a for $t_a = 13$ h and with annealing time t_a at $T_a = 475$ K are presented in Figs. 4 and 5, respectively, where the data of the as-quenched samples are also shown for comparison. The heating curve of the annealed sample, $C_{p,a}$, shows a $C_p(T)$ behaviour which closely follows the specific curve of the reference sample, $C_{p,s}$, up to each annealing temperature, and then exhibits an excess endothermic peak relative to the reference sample before merging with that of the as-quenched sample at a temperature below $T_g = 645$ K where T_g is defined as the point of inflection in the $C_p(T)$ curve.

The significant features of Figs. 4 and 5 may be summarized as follows:

1. The sample annealed at T_a shows an excess endothermic reaction beginning at T_a, implying that the $C_{p,a}$ curve in the temperature range above T_a is dependent on the thermal history and consists of configurational contributions as

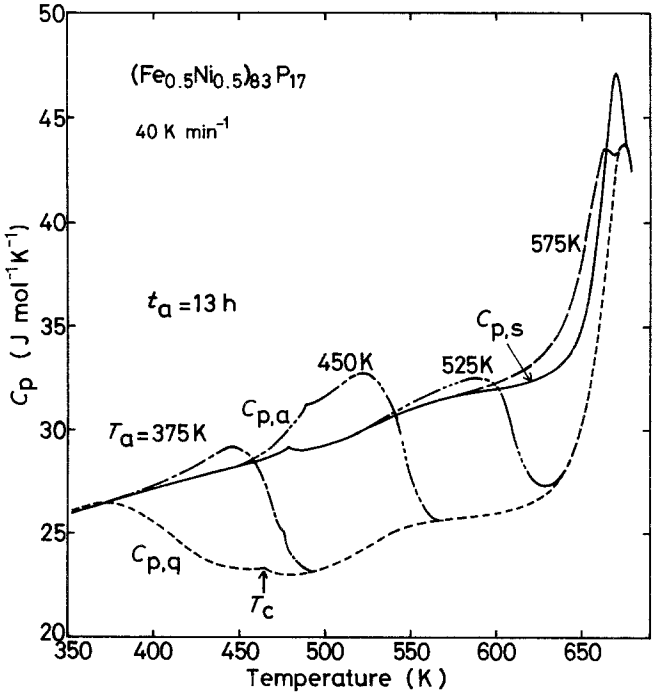

Figure 4 The thermograms of an amorphous $(Fe_{0.5}Ni_{0.5})_{83}P_{17}$ alloy subjected to anneals for 13 h at various temperatures from 375 to 575 K. The solid line presents the thermogram of the sample subjected to heating to 675 K.

well as those arising from purely thermal vibrations. Therefore, the vibrational specific heat, $C_{p,v}$ for the Fe–Ni–P amorphous alloy was extrapolated from C_p values in the low temperature region $T \leqslant 450$ K and is a linear function of temperature such that

$$C_{p,v} = 28.2 + 2.4 \times 10^{-2} (T - 450) \text{ J mol}^{-1} \text{ K}^{-1} \quad (1)$$

However, the equilibrium specific heat, $C_{p,e}$, of the supercooled liquid including the vibrational and configurational specific heat could not be determined owing to the crystallization at a temperature just above T_g($\simeq$ 675 K).

2. The excess endothermic curves always begin to rise at T_a, being independent on the annealing time. Furthermore, both the magnitude and the

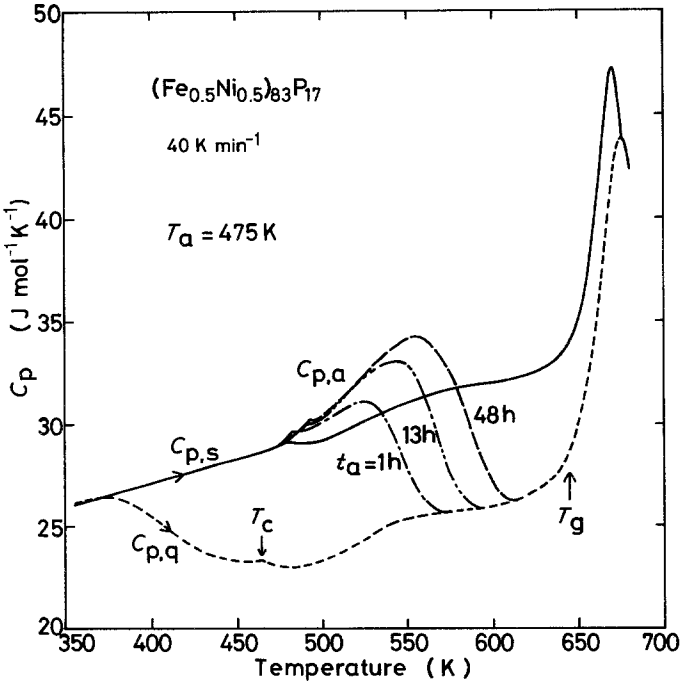

Figure 5 The thermograms of an amorphous $(Fe_{0.5}Ni_{0.5})_{83}P_{17}$ alloy subjected to anneal at 475 K for various periods from 1 to 48 h. The solid line presents the thermogram of the sample subjected to heating to 675 K.

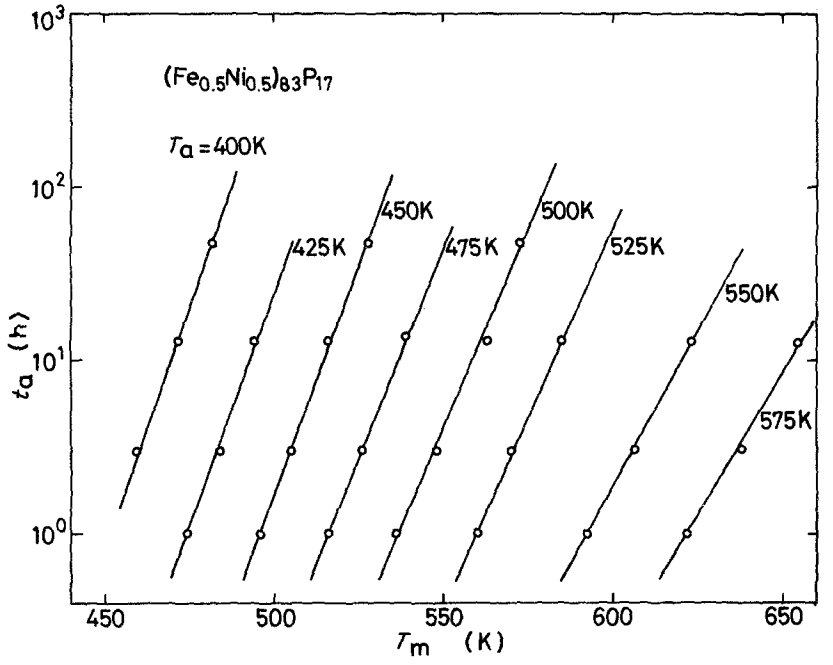

Figure 6 Variation of the $\Delta C_p = C_{p,a} - C_{p,s}$ peak temperature, T_m, as a function of annealing time t_a for an amorphous $(Fe_{0.5}Ni_{0.5})_{83}P_{17}$ alloy annealed at various temperatures from 400 to 575 K.

temperature of the endothermic peak tend to increase linearly with the logarithm of the time ($\ln t_a$), as plotted in Fig. 6.

3. The excess endothermic peak is reversible while the exothermic broad peak is irreversible and the $C_p(T)$ curve of the annealed samples couples the reversible endothermic and irreversible exothermic reaction.

4. If the annealing is performed at temperatures well below $T_g(T_a \leqslant 550\,K)$, it does not affect the glass transition process. This is indicated by the close overlap of $C_p(T)$ curves for the annealed and unannealed samples at temperatures below T_g.

Quite similar $C_{p,a}(T)$ curves as a function of T_a and/or t_a were recognized for $(Fe_{0.5}Ni_{0.5})_{83}B_{17}$ amorphous samples and the thermograms as a function of T_a for $t_a = 13\,h$ and t_a at $T_a = 500\,K$ are shown in Figs. 7 and 8, respectively. The

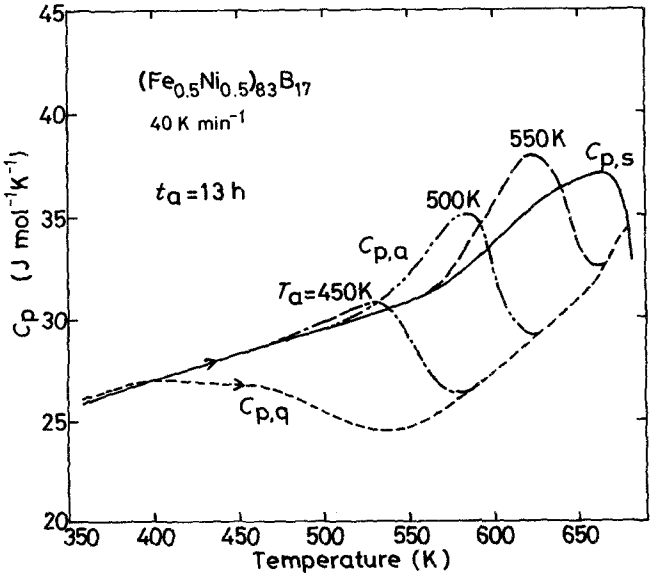

Figure 7 The thermograms of an amorphous $(Fe_{0.5}Ni_{0.5})_{83}B_{17}$ alloy subjected to anneals for 13 h at various temperatures from 450 to 550 K. The solid line presents the thermogram of the sample subjected to heating to 665 K.

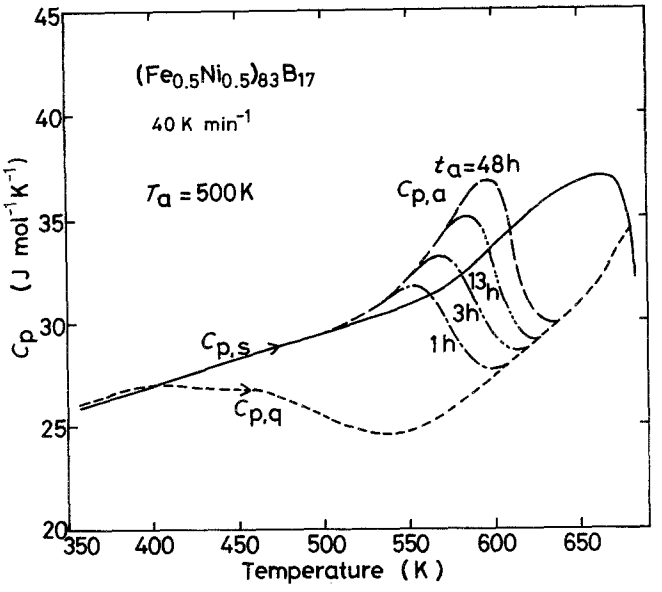

Figure 8 The thermograms of an amorphous $(Fe_{0.5}Ni_{0.5})_{83}B_{17}$ alloy subjected to anneals at 500 K for various periods from 1 to 48 h. The solid line represents the thermogram of the sample subjected to heating at 665 K.

vibrational specific heat, $C_{p,v}$, of the Fe–Ni–B alloy, which was determined by extrapolating the C_p values in the low temperature region $T \leqslant 500$ K, is presented by the following linear function of temperature.

$$C_{p,v} = 29.4 + 2.6 \times 10^{-2} (T - 500) \text{ J mol}^{-1} \text{ K}^{-1} \quad (2)$$

Fig. 9 also shows that the temperature of the endothermic peak for the Fe–Ni–B alloy increases linearly with the logarithm of the time ($\ln t_a$), similar to that for the Fe–Ni–P alloy. The temperature dependence of the $C_{p,v}$ is larger by about 8% for the Fe–Ni–B alloy than for the Fe–Ni–P alloy. From the features derived from Figs. 4 to 9, the too strict separation of the relaxation process into chemical short-range order and topological shirt-range order, which was previously proposed, is thought to be over simplified. Alternatively it was suggested that the reversible relaxation arises from compositional short-range localized relaxation regions of the more less rigid matrix while the irreversible structural relaxation results from the annihilation of various kinds of quenched-in "defects" as well as the topological and compositional atomic regroupings. The further discussion of this point will be described in Section 4.

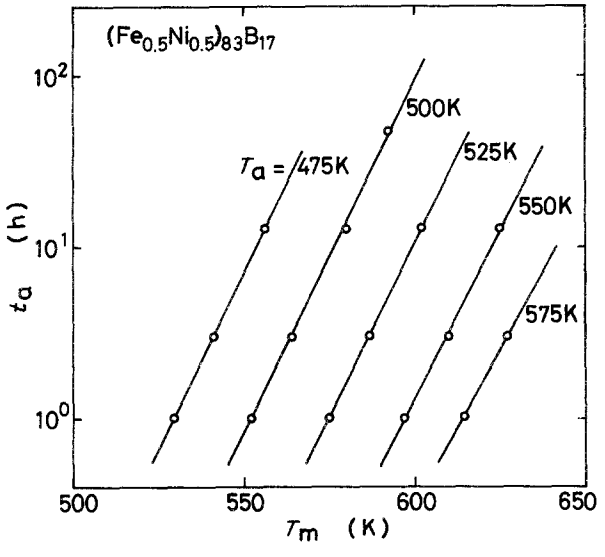

Figure 9 Variation of the $\Delta C_p = C_{p,a} - C_{p,s}$ peak temperature, T_m, as a function of annealing time t_a for an amorphous $(Fe_{0.5}Ni_{0.5})_{83}B_{17}$ alloy annealed at various temperatures from 475 to 575 K.

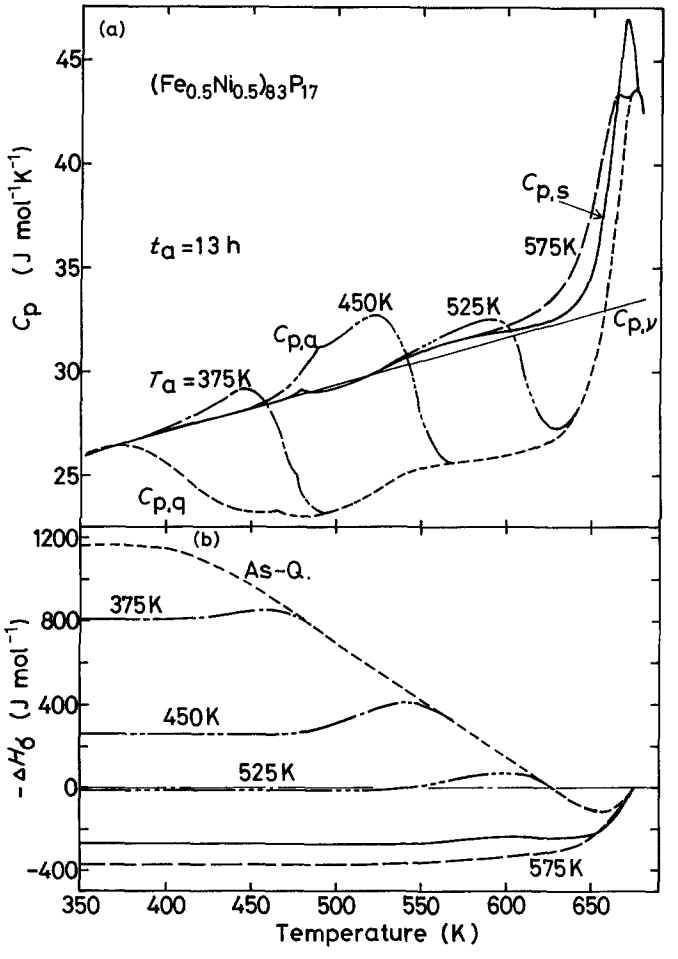

Figure 10 (a) The endothermic peak of an amorphous $(Fe_{0.5}Ni_{0.5})_{83}P_{17}$ alloy subjected to anneals for 13 h at various temperatures ranging from 375 to 575 K. (b) The change in the configuration enthalpy $\Delta H_\sigma(T)$ corresponding to the appearance of the endothermic peak, where ΔH_σ (675 K) is set to zero.

3.3. Configuration enthalpy, $\Delta H_\sigma(T)$, of annealed samples

The change in the configuration enthalpy, $\Delta H_\sigma(T)$, upon annealing at T_a for t_a for the $(Fe_{0.5}Ni_{0.5})_{83}P_{17}$ amorphous alloy which was evaluated from $C_p(T)$ data shown in Figs. 4 and 5 is shown in Figs. 10 and 11. Here the configuration enthalpy at 675 K was taken to be the reference with $\Delta H_\sigma(675\,K) = 0$, and the relaxed configurational enthalpy $\Delta H_\sigma(T)$ was expressed by:

$$\Delta H_\sigma(T) = \int_{675}^{T} (C_{p,a} - C_{p,\nu})dT \qquad (3)$$

As seen in the figures, the configurational enthalpy curve falls progressively with the annealing time and annealing temperature, indicating that the low-temperature anneals stabilize the amorphous structure. With rising temperature, the ΔH_σ of the annealed sample increases towards the reference value and merges with it before the complete transition of amorphous solid to supercooled liquid, implying that it is possible to recover the initial structure of the amorphous alloy without reheating above T_g. This feature differs significantly from the common phenomenon [8–10] that the ΔH_σ of the amorphous materials annealed in a temperature range slightly below T_g changes significantly even after the glass transition.

3.4. Changes in $\Delta C_{p,r,endo}$ and $\Delta H_{r,endo}$ with T_a and t_a

With an aim to clarify the effects of T_a and t_a on the magnitude of the endothermic peak, the temperature dependence of the differences in C_p between annealed (T_a = 350 to 600 K, t_a = 1, 3, 13, 48 h) and the reference states, $[\Delta C_{p,r,endo} = C_{p,a}(T) - C_{p,s}(T)]$, is shown in Fig. 12 for $(Fe_{0.5}Ni_{0.5})_{83}P_{17}$ and Fig. 13 for $(Fe_{0.5}Ni_{0.5})_{83}B_{17}$. These figures reveal the following features: firstly, the change in the magnitude of the $\Delta C_{p,r,endo}$ with T_a is not monotonic and shows two separable maxima which peak respectively at T_a = 450 K and T_a = 575 to 600 K for the Fe–Ni–P samples and at T_a = 550 K and T_a = 600 to 625 K for the

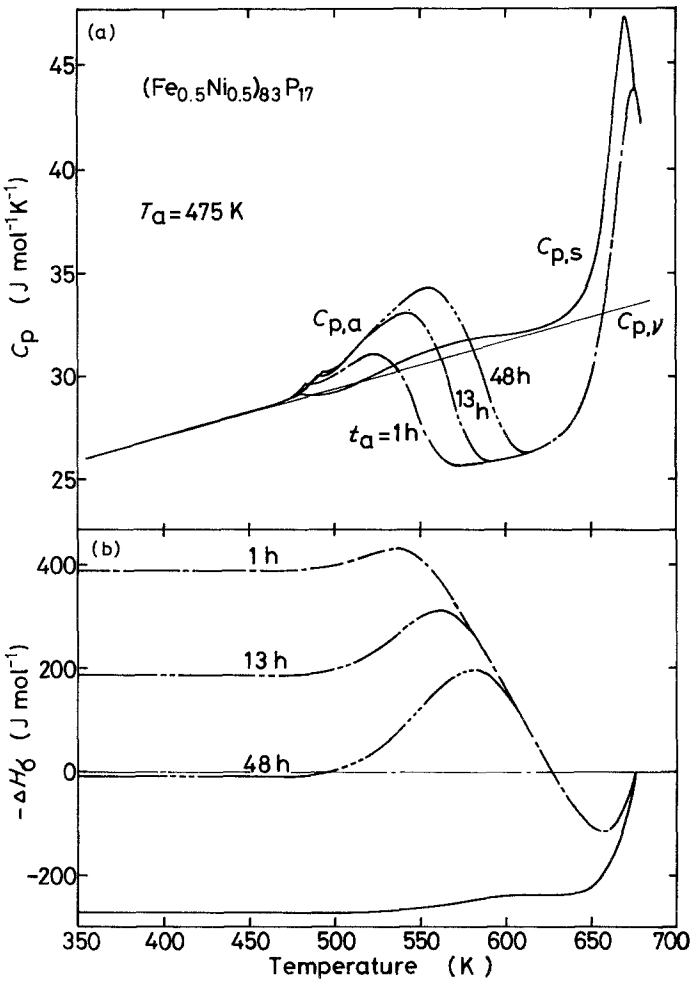

Figure 11 (a) The endothermic peak of an amorphous $(Fe_{0.5}Ni_{0.5})_{83}P_{17}$ alloy subjected to anneals at 475 K for various periods from 1 to 48 h. (b) The change in the configuration enthalpy $\Delta H_\sigma(T)$ corresponding to the appearance of the endothermic peak, where ΔH_σ (675 K) is set to zero.

Fe–Ni–B samples, indicating that the anneal-induced enthalpy relaxation occurs by two separate mechanisms. Secondly, the magnitude of the $\Delta C_{p,r,endo}$ increases with t_a in a continuous manner in the temperature ranges ($T_a \leqslant 450$ K and $T_a = 550$ to 600 K for the Fe–Ni–P alloy and $T_a \leqslant 550$ K and $T_a = 600$ K for the Fe–Ni–B alloy) where the evolution of the reversible endothermic peak is attributed to individual single mechanism for structural relaxation. Thirdly, while the maximum value of $\Delta C_{p,r,endo}$ is nearly equal for both the alloy systems, the temperature range where the endothermic reactions occurs is lower by about 75 to 100 K for the Fe–Ni–P alloy than that for the Fe–Ni–B alloy, indicating that the reversible structural relaxation in a low temperature range occurs more easily for the Fe–Ni–P alloy, similar to the result (Figs. 1 to 3) of the irreversible structural relaxation.

Figure 14 shows the change in enthalpy relaxation $\Delta H_{r,endo}$ as a function of annealing time at $T_a = 400$, 425, 450, 550 and 575 K for $(Fe_{0.5}Ni_{0.5})_{83}P_{17}$ and at $T_a = 475$, 500 and 525 K for $(Fe_{0.5}Ni_{0.5})_{83}B_{17}$. Here

$$\Delta H_{r,endo}(T_a, t_a) = \int \Delta C_p(T)(= C_{p,a} - C_{p,s})dT$$

$$\Delta C_p(T) \geqslant 0 \qquad (4)$$

$\Delta H_{r,endo}(T_a)$ of both the alloys increases with $(\ln t_a)^n$ ranging from 1 to 2 and the n value tends to decrease with rising T_a. This $\ln t_a$ dependence of $\Delta H_{r,endo}(T_a)$ is expected as both the magnitude and temperature of the ΔC_p peak scale nearly as $\ln t_a$ (see Figs. 6 and 9), being the same as those by low temperature annealing for $Pd_{48}Ni_{32}P_{20}$ [6] and (Fe, Co, Ni)$_{75}Si_{10}B_{15}$ [5] alloys.

The changes in the maximum differential specific heat, $\Delta C_{p,max} = C_{p,a} - C_{p,s}$, and the enthalpy relaxation, $\Delta H_{r,endo}$, during annealing for different periods (t_a) as a function of T_a are

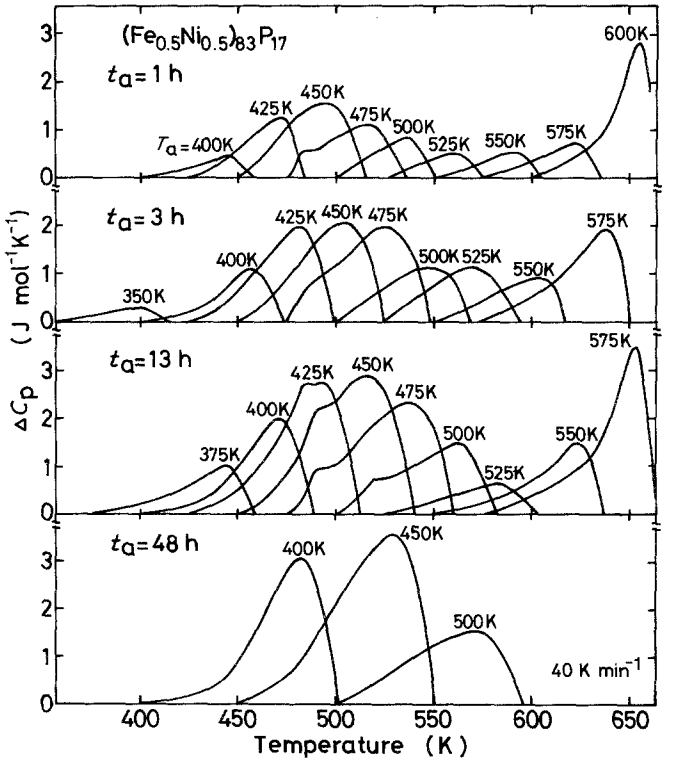

Figure 12 The differential specific heat $\Delta C_p(T)$, between the reference and annealed samples for an amorphous $(Fe_{0.5}Ni_{0.5})_{83}P_{17}$ alloy subjected to anneals at various temperatures ranging from 400 to 600 K for different periods from 1 to 48 h.

shown in Fig. 15 for $(Fe_{0.5}Ni_{0.5})_{83}P_{17}$ and Fig. 16 for $(Fe_{0.5}Ni_{0.5})_{83}B_{17}$. With increasing T_a, both the values $\Delta C_{p,max}$ and $\Delta H_{r,endo}$ increase at first, show maximum values at about 450 K for the Fe–Ni–P alloy and at about 525 K for the Fe–Ni–B alloy, and then decrease significantly in the range from 450 to 550 K for the former alloy and from 525 to 575 K for the latter alloy followed by a rapid increase at temperatures slightly below T_g. The distinct splitting of the peaks of the $\Delta C_{p,max}(t_a)$ and $\Delta H_{r,endo}(t_a)$ as a function of T_a indicates clearly that the enthalpy relaxation of the

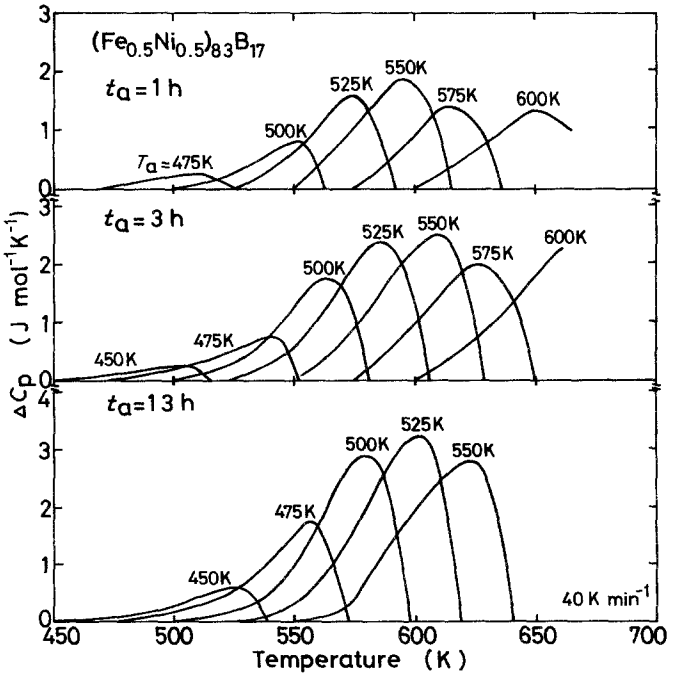

Figure 13 The differential specific heats, $\Delta C_p(T)$, between the reference and annealed samples for an amorphous $(Fe_{0.5}Ni_{0.5})_{83}B_{17}$ alloy subjected to anneals at various temperatures ranging from 450 to 600 K for different periods for 1 to 13 h.

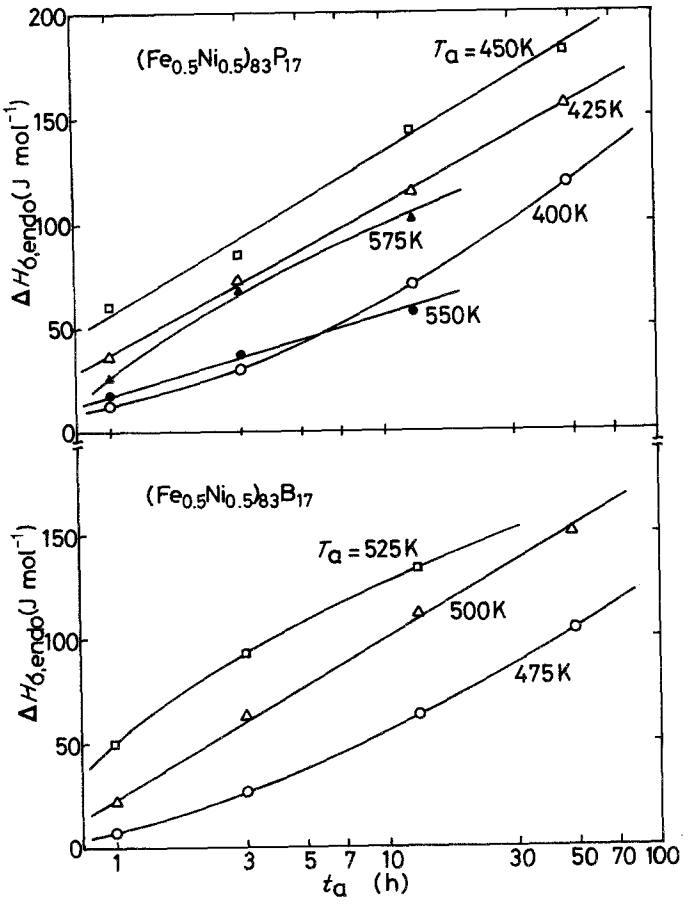

Figure 14 The variation of the enthalpy relaxation, $\Delta H_{\sigma,endo}$, as a function of annealing time t_a for amorphous $(Fe_{0.5}Ni_{0.5})_{83}P_{17}$ and $(Fe_{0.5}Ni_{0.5})_{83}B_{17}$ alloys at various temperatures ranging from 400 to 575 K.

amorphous alloys on annealing occurs by two distinguishable mechanisms. The rapid increases in the $\Delta C_{p,max}$ and $\Delta H_{r,endo}$ at temperatures above 550 K for the Fe–Ni–P alloy and above 575 K for the Fe–Ni–B alloy are interpreted to correspond to the common glass transition phenomena. Accordingly, the annealing temperature range can be divided for convenience into the following two regions; (1) the first stage region in the range of $T_a < T_g - 120$ K, and (2) the second region in the range of $T_g - 120 < T_a < T_g$. It is worthy to point out that the $\Delta C_{p,max}(T_a)$ and $\Delta H_{r,endo}(T_a)$ behaviour of the annealed samples is similar to the exothermic $\Delta C_p(T)$ behaviour of the as-quenched sample shown in Fig. 3 regarding the appearance of the two-stage relaxation and their peak temperatures. The similarity suggests that the reaction mechanisms at each stage for the irreversible and the reversible structural relaxations are similar.

Furthermore, it is very important to point out that a similar two-stage splitting of the endothermic peak is seen even for the $(Fe_{0.5}Ni_{0.5})_{83}P_{17}$ samples annealed for t_a at T_a after preannealing for 1 min at 640 K as exemplified in Fig. 17, in addition to the case of the samples annealed after melt-quenching. However, the magnitude of the $\Delta C_{p,endo}$ peak of the preannealed samples is smaller by about 40% than that of the as-quenched samples and the annealing temperature at which the $\Delta C_{p,max}$ of the first-stage reaction exhibits a maximum value increases from $\simeq$ 450 K for the as-quenched sample to $\simeq$ 475 K for the preannealed sample. Such differences in the $\Delta C_{p,endo}$ peak behaviour between the as-quenched and the preannealed samples have been also recognized for $Pd_{48}Ni_{32}P_{20}$ alloy [6].

3.5. Change in Curie temperature with T_a and t_a

It has been reported that the irreversible and reversible structural relaxations cause significant changes in physical and mechanical properties such as internal friction [11–14], ferromagnetic Curie temperature [15–18], Young's modulus, [19–21], electrical resistance [22–24], superconducting critical temperature [25–29], and fracture

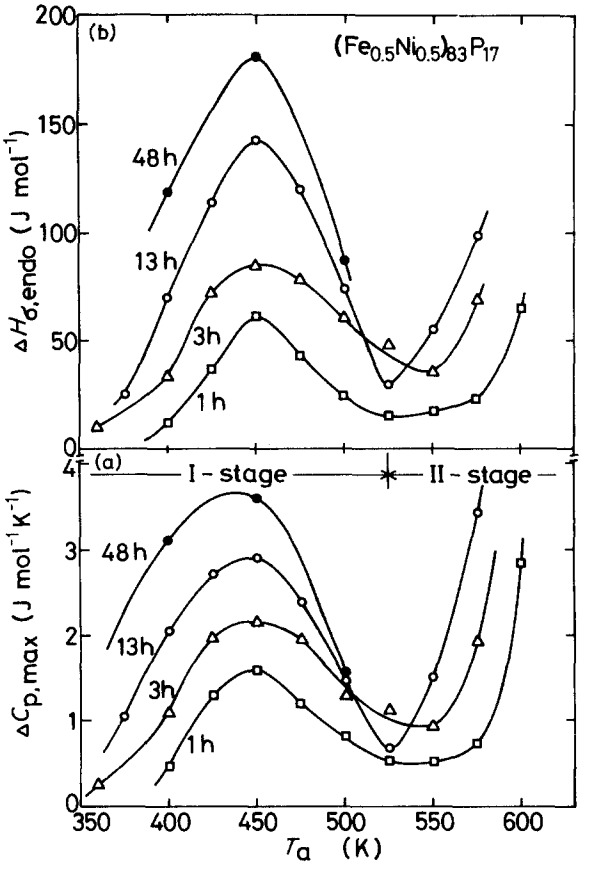

Figure 15 The variations of the maximum differential specific heat $\Delta C_{p,max}$ (a) and the enthalpy relaxation, $\Delta H_{\sigma,endo}$ (b) as a function of annealing temperature for an amorphous $(Fe_{0.5}Ni_{0.5})_{83}P_{17}$ alloy subjected to anneals for different periods from 1 to 48 h.

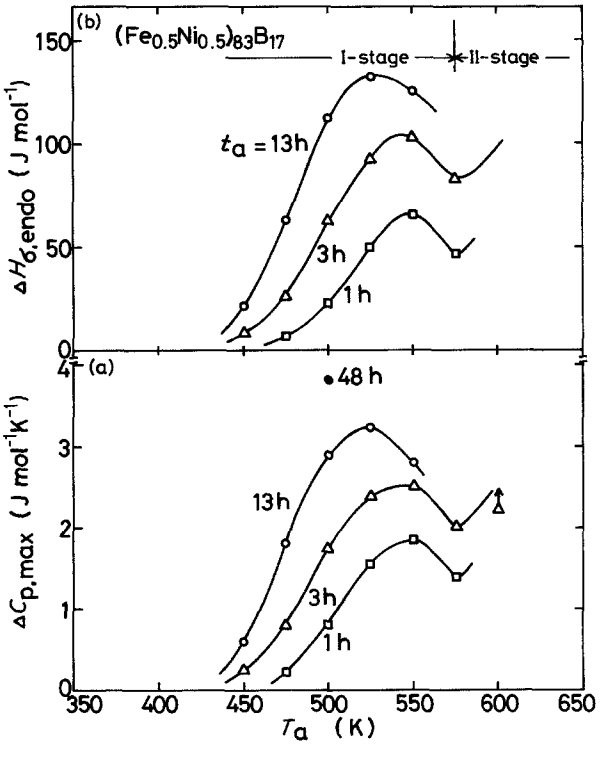

Figure 16 The variations of the maximum differential specific heat, $\Delta C_{p,max}$ (a) and the enthalpy relaxation, $\Delta H_{\sigma,endo}$ (b) as a function of annealing temperature for an amorphous $(Fe_{0.5}Ni_{0.5})_{83}B_{17}$ alloy subjected to anneals for different periods from 1 to 48 h.

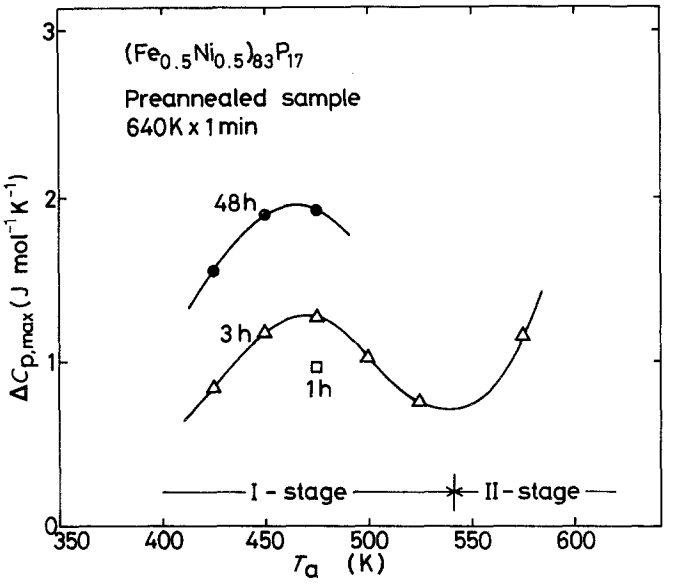

Figure 17 The variation of the maximum differential specific heat, $\Delta C_{p,max}$, as a function of annealing temperature for an amorphous $(Fe_{0.5}Ni_{0.5})_{83}P_{17}$ alloy subjected to anneals for 3 and 48 h at various temperatures after preannealing for 1 min at 640 K.

strain [30, 31] etc. Although the low-temperature annealing is well known to result in an irreversible and reversible rise of T_c, there is no information on the correlation between T_c and the double-stage enthalpy relaxations. It is strongly expected that the clarification of the mutual relationship offers a valuable information for the interpretation of the mechanisms of the two-stage reaction. Fig. 18 shows the change of T_c for $(Fe_{0.5}Ni_{0.5})_{83}P_{17}$ amorphous samples on annealing at T_a for t_a. The T_c is 465 K in as-quenched state and rises irreversibly to 480 K after heating to 640 K which is nearly equal to T_g. On annealing the sample (preheated to 640 K) at 475 K for 3 h, T_c rises further to 486 K and the subsequent heating to 640 K results in a lowering of T_c to the previous value (480 K), i.e. T_c of the sample heated previously to 640 K changes reversibly. The amplitude of the change in T_c depends on both T_a and t_a. Furthermore, it is noted in Fig. 18 that T_c rises in the case of

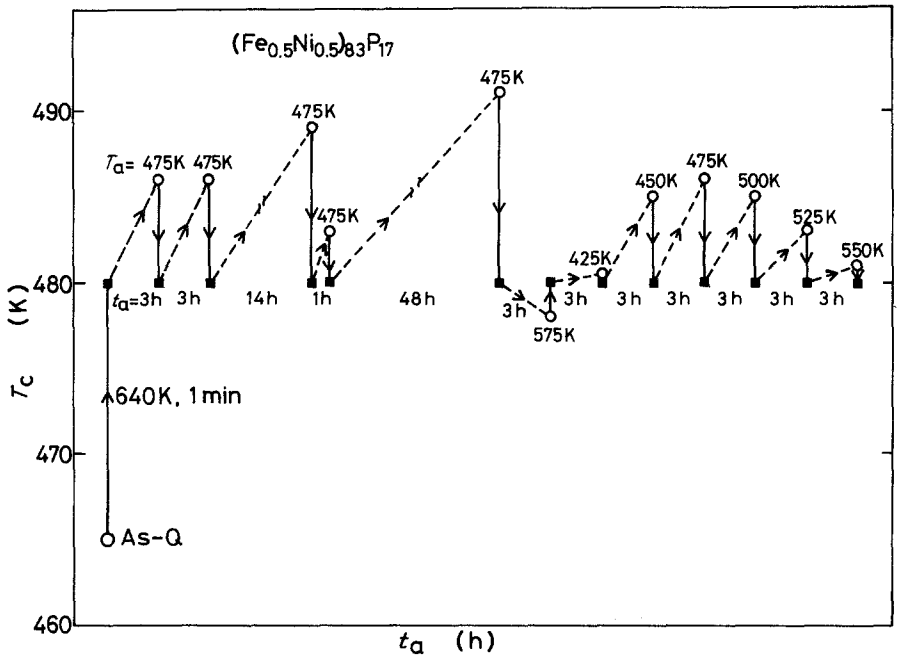

Figure 18 The change in the Curie temperature T_c for an amorphous $(Fe_{0.5}Ni_{0.5})_{83}P_{17}$ alloy subjected to anneals at various temperatures ranging from 425 to 575 K for different periods from 3 to 48 h.

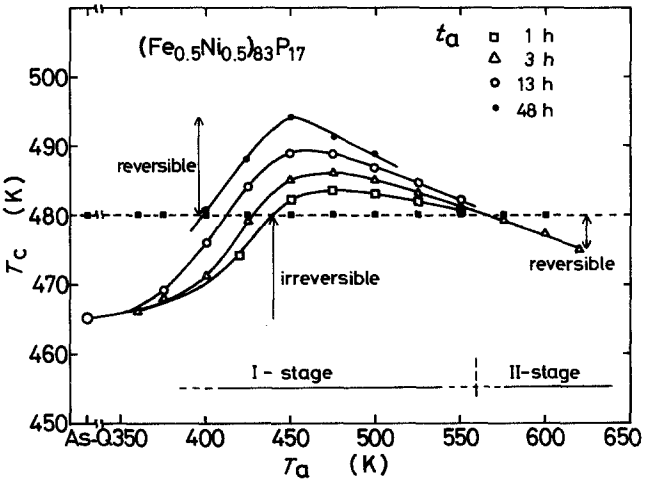

Figure 19 The variation of the Curie temperature T_c as a function of annealing temperature for an amorphous $(Fe_{0.5}Ni_{0.5})_{83}P_{17}$ alloy subjected to anneals for different periods form 1 to 48 h.

$T_a \leqslant 500\,K$ and lowers in the case of $T_a > 550\,K$. Based on the data of Fig. 18, the T_c values for various t_a values as a function of T_a are plotted in Fig. 19. It is seen that the change in T_c with T_a can be distinguished as following two stages: (1) a reversible rise of T_c from 480 K to various values at $400\,K \leqslant T_a \leqslant 550\,K$; and (2) a reversible lowering of T_c from 480 K to various values at $550\,K < T_a \leqslant 625\,K$. Furthermore, Fig. 19 shows that the T_a at which T_c exhibits a maximum value tends to decrease with t_a from 475 K for $t_a = 1$ h to 450 K for $t_a = 48$ h.

4. Discussion

4.1. Activation energy for enthalpy relaxation $Q_m(T_m)$

The information on the activation energy for structural relaxation can be obtained from the data of the change of T_m either by isothermal annealing or continuous heating. If the $\Delta C_{p,r,endo}$ peak at T_m is associated with a relaxation entity, an apparent activation energy for enthalpy relaxation, Q_m, of $(Fe_{0.5}Ni_{0.5})_{83}P_{17}$ and $(Fe_{0.5}Ni_{0.5})_{83}B_{17}$ amorphous alloys can be evaluated from isothermal annealing data of Figs. 6 and 9 by using the following relation [32],

$$Q_m(T_m)/k_B = d \ln t_a^*/d(1/T_a) \qquad (5)$$

where t_a^* is the annealing time for the appearance of $\Delta C_{p,max}$ at T_m and k_B is Boltzmann's constant. Figs. 20 and 21 show a plot of $\log t_a$ against $1/T_a$ for the first stage (○) and the second stage (●) peaks of $(Fe_{0.5}Ni_{0.5})_{83}P_{17}$ and $(Fe_{0.5}Ni_{0.5})_{83}B_{17}$ amorphous samples. A rather good linear relation for each peak, indicating the satisfaction of an Arrhenius temperature dependence is seen. As plotted in Fig. 22, $Q_m(T_m)$ of the Fe–Ni–P alloy is not constant and increases with increasing T_m from 1.7 eV at $T_m = 475\,K$ to 2.5 eV at $T_m = 600\,K$ for the first stage peak and from 2.6 eV at 600 K to 5.0 eV at 650 K for the second stage peak. Similarly, the $Q_m(T_m)$ of the Fe–Ni–B alloy tends to increase with T_m from 1.8 eV at 560 K to 2.0 eV at 620 K, but the degree of the change in Q_m with T_m is considerably smaller as compared with the case of the Fe–Ni–P alloy.

Alternatively, $Q_m(T_m)$ was evaluated from the shift in the $\Delta C_{p,r,endo}$ spectrum with scanning rate, α, from equation 6 [33, 34] as exemplified in Fig. 23.

$$Q_m(T_m)/k_B \simeq \frac{d \ln (T_m^2/\alpha)}{d(1/T_m)} = -2T_m - \frac{d \ln \alpha}{d(1/T_m)} \simeq \frac{d \ln \alpha}{d(1/T_m)} \qquad (6)$$

where $T \ll Q_m/k_B$. The Q_m values thus evaluated are nearly equal to those obtained from the isothermal data as seen in Fig. 22.

The observed Q_m increases rather drastically by the change of the first-stage peak to the second-stage peak. The relatively small $Q_m(T_m)$ values in the first stage reflect the occurrence of local and/or medium range structural relaxation while the large $Q_m(T_m)$ values in the second stage are attributed to that of cooperative structural relaxation.

The activation energy Q_m has the following relation to the frequency factor ν_0 and T_m if the first order rate reaction process for the enthalpy relaxation is assumed.

$$Q_m = k_B T_a \ln \nu_0 t_a^* = k_B T_m \ln \nu_0 \tau^* = Q_m(T_m) \qquad (7)$$

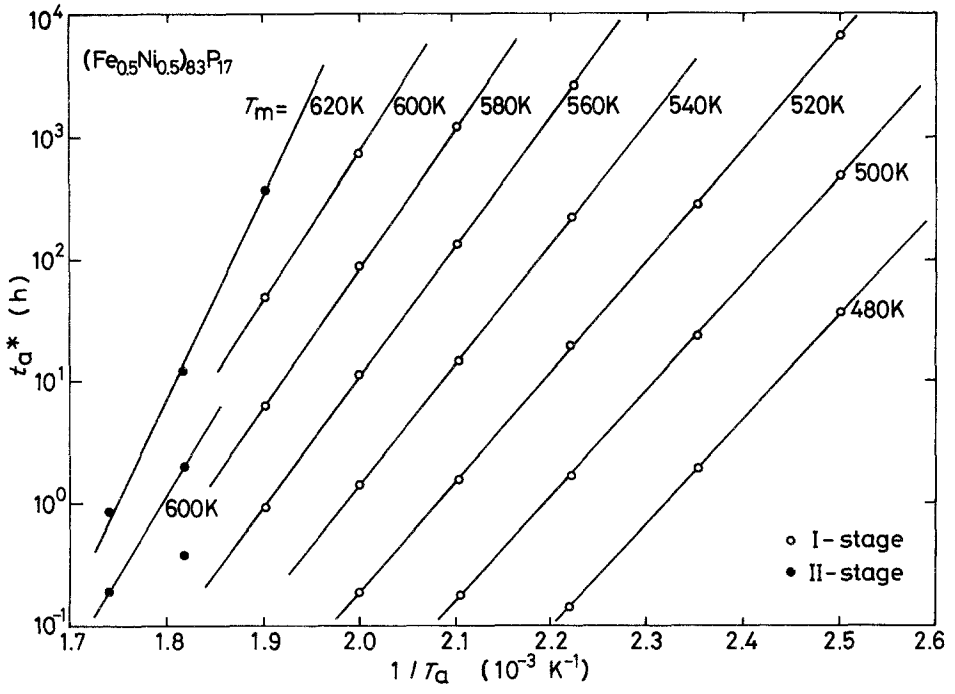

Figure 20 The annealing time, t_a^*, for the appearance of the ΔC_p peak at T_m as a function of the inverse of the annealing temperature $1/T_a$ for an amorphous $(Fe_{0.5}Ni_{0.5})_{83}P_{17}$ alloy.

Here τ^* is the relaxation time at T_g and is related to the scanning rate $\alpha = 2/3\,K\,sec^{-1}$ such that $\tau^* = k_B T_m^2/Q_m\alpha \simeq 30$ sec [35]. The frequency factor $\nu_0(T_m)$ calculated from Equation 7 is plotted in Fig. 22. The ν_0 of the Fe–Ni–P alloy increases with T_m from $\simeq 10^{16}\,sec^{-1}$ at 475 K to $\simeq 10^{19}\,sec^{-1}$ at 650 K for the second stage reaction, while there is no appreciable change in ν_0 value of the Fe–Ni–B alloy as a function of T_m. These ν_0 values are somewhat higher than Debye frequency $\nu_D \simeq 10^{13}$ to $10^{14}\,sec^{-1}$ for the first-stage relaxation and much higher for the second stage relaxation. Fig. 20 also shows that both the values of $Q_m(T_m)$ and ν_0 are larger for the Fe–Ni–P alloy than for the Fe–Ni–B alloy.

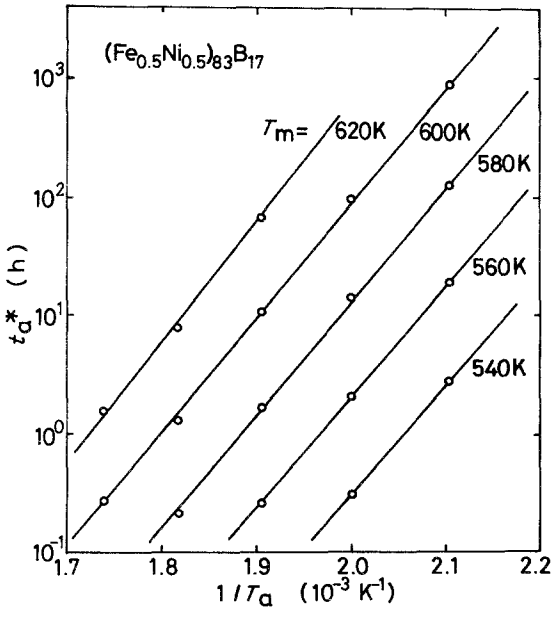

Figure 21 The annealing time, t_a^*, for the appearance of the ΔC_p peak at T_m as a function of the inverse of the annealing temperature $1/T_a$ for an amorphous $(Fe_{0.5}Ni_{0.5})_{83}B_{17}$ alloy.

4.2. Anneal-induced relaxation spectra

In a previous section, the activation energy for enthalpy relaxation was found to exhibit a broad two-stage distribution against T_m. Based on Primak's theory [36] on the kinetics of processes distributed in activation energy, the enthalpy relaxation spectrum as a function of T_m has been evaluated by Chen [16]. According to his analyses, the relaxation spectrum $\Delta C_{p,endo}(T)$ is evaluated from Equation 8.

$$C_{p,endo}(T) = N_0(T)\gamma(T) \qquad (8)$$

where $N_0(T)$ is the distribution of the relaxation entity, and $\gamma(T)$ is the coupling strength contributing to the specific heat $\Delta C_{p,endo}$. As $\gamma(T) \propto$

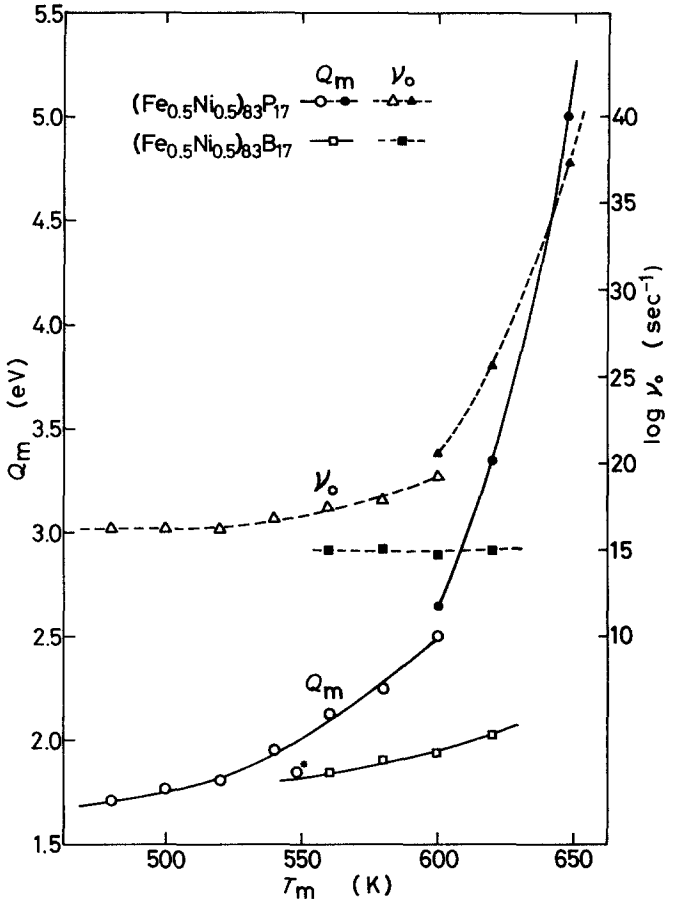

Figure 22 The activation energy spectrum, $Q_m(T_m)$ and the frequency factor, $\nu_0(T_m)$ as a function of T_m for amorphous $(Fe_{0.5}Ni_{0.5})_{83}P_{17}$ and $(Fe_{0.5}Ni_{0.5})_{83}B_{17}$ alloys.

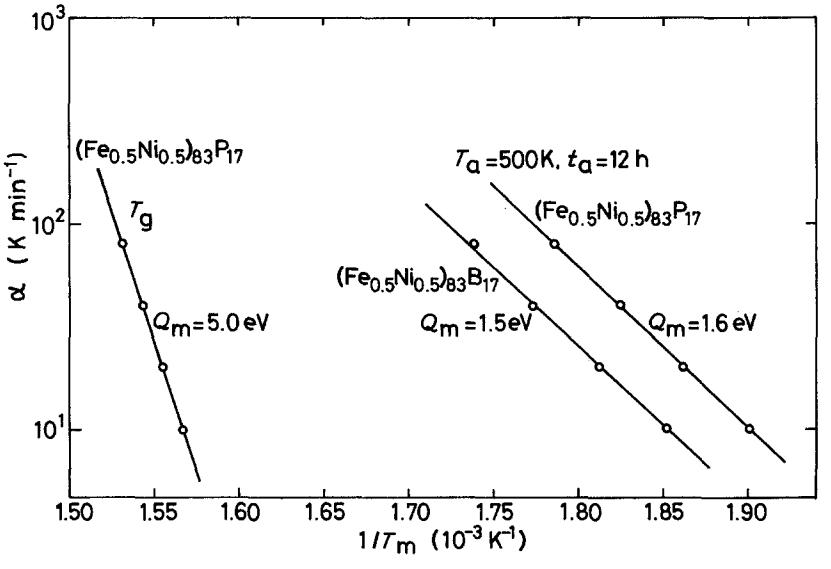

Figure 23 Ozawa plots of ln α against $1/T_m$ for amorphous $(Fe_{0.5}Ni_{0.5})_{83}P_{17}$ and $(Fe_{0.5}Ni_{0.5})_{83}B_{17}$ alloys.

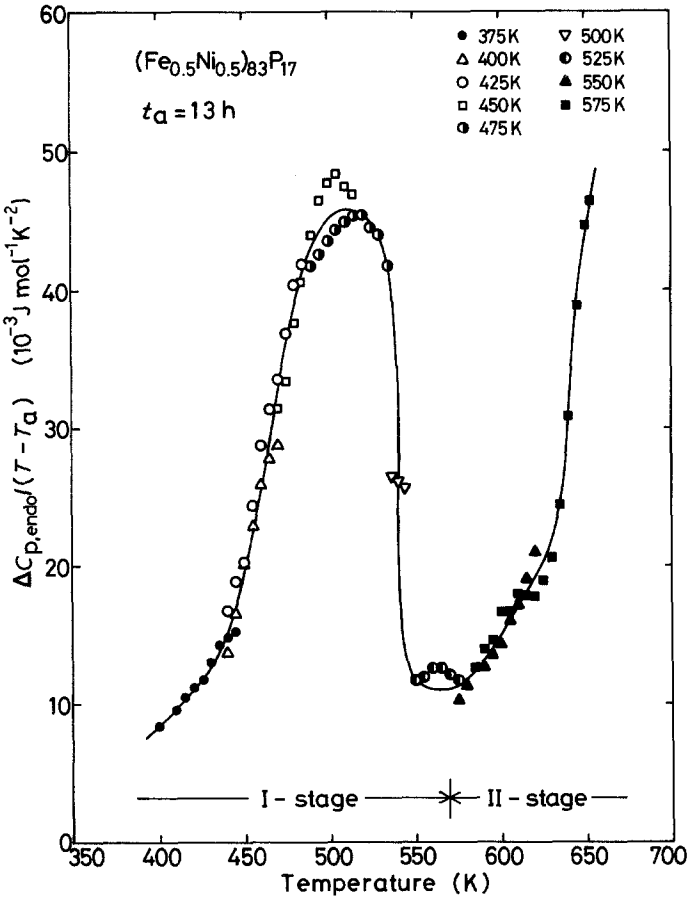

Figure 24 The relaxation entity spectra, $N_0(T) \simeq C_{p,endo}(T)/(T - T_a)$ for an amorphous $(Fe_{0.5}Ni_{0.5})_{83}P_{17}$ alloy as a function of temperature.

$(T - T_a)$, Equation 9 reduces to

$$N_0(T) \propto \Delta C_{p,endo}(T)/(T - T_a). \quad (9)$$

$N_0(T)$ values of $(Fe_{0.5}Ni_{0.5})_{83}P_{17}$ alloy evaluated from the data of $\Delta C_{p,endo}(T)$ shown in Fig. 12 are plotted in Fig. 24. It is seen that $N_0(T)$ also shows two separatable maxima, which peak respectively at 500 K and T_g, and reproduces fairly well the actually measured distribution of the maximum $\Delta C_{p,endo}$ as a function of T_a shown in Fig. 15. The good reproducibility enables us to conclude clearly that the relaxation entity for $(Fe_{0.5}Ni_{0.5})_{83}P_{17}$ amorphous alloy distributes at two stages against T_a and t_a. Judging from the result that the T_a dependence of the $\gamma(T)$ and the relatively large frequency factor $\nu_0 \gg \nu_D$ are similar to the relaxation behaviour commonly observed for anneal at temperatures just below T_g, each spectrum of the first-stage and the second-stage relaxations is therefore thought to be attributed phenomenologically to a distribution of two kinds of characteristic glass transitions (T_{g1} and T_{g2}) with an apparent activation energy Q_1 and Q_2.

4.3. Interpretation of the two-stage enthalpy relaxation phenomena

In the framework of a percolation process which was conceived by Cohen and Grest [37] and Cyat [38], the model for the appearance of the reversible endothermic peak in the annealed amorphous samples has been proposed. Cyat [38] and Chen [6] have proposed that a supercooled liquid structure near T_g is inhomogenous and consists of liquid-like regions of large free volume or high local free energy and solid-like regions with small free volume or low local free energy. The resulting amorphous solid prepared by melt-quenching contains a number of liquid-like regions with unrelaxed atomic configuration which are isolated from each other embedded in the solid-like matrix. The inhomogeneity for an alloy is considered to arise from fluctuations in concentration and density. When the amorphous solid is annealed at T_a for t_a, a part of liquid-like regions undergo configurational change to a relaxed state by the independent and noncooperative manner. However, the local structural relaxation itself in

the cluster involving several atoms can be cooperative. The sizes of the cluster have been approximated to be 1 to 2 nm. Each liquid-like region, m, manifests a liquid-amorphous transition at T_{gm} which depends on the atomic configuration state. The difference in specific heat, $\Delta C_{p,g}(T) = C_{p,s}(T) - C_{p,\nu}(T)$ (see Figs. 4, 5, 7 and 8), then would represent the distribution of the glass transition $T_{g,m}$.

When an amorphous alloy is annealed at temperatures well below T_g, the regions with characteristic relaxation times, τ_m, given by Equation 10, being shorter than the duration of annealing t_a, would undergo local relaxation towards the local equilibrium states at T_a.

$$\tau_m \simeq \tau_{mea} \exp\left[-\frac{Q_m}{k_B}(1/T_a - 1/T_{g,m})\right] \quad (10)$$

Here τ_{mea} is the time constant of measurements. Each local relaxation contributes to the enthalpy relaxation proportional to $(T_{g,m} - T_a)$. Upon heating the annealed sample, each region, m, recovers the initial structure (the so-called "reversion") and contributes to an excess endothermic specific heat as the local amorphous-liquid transition occurs at or slightly above $T_{g,m}$. Thus the peak temperature of the $\Delta C_{p,endo}$ evolves in a continuous manner against the logarithm of t_a with intensity proportional to $(T_{g,m} - T_a)N_0(T_{g,m})$.

Recently, Chen and Morito [39, 40] proposed an extended free-volume model to interpret the internal friction data of bulk-shaped Pd–Cu–Si, Pd–Ni–P and Pt–Ni–P amorphous alloys. In the model, it is assumed that (1) there exists in an amorphous alloy a fluctuation in the frozen-in local free-volume with the probable distribution of total free volume v_f,

$$P(v) = \frac{\gamma}{v_f} \exp(-\gamma v/v_f), \quad (11)$$

(2) internal friction arises from relaxation within localized structural entity of double-well potential, and (3) the activation energy for the relaxation is simply related to the activation energy that

$$Q \propto Q_0\left(1 - \frac{v}{v^*}\right) \quad (12)$$

with a relaxation time

$$\tau = \tau_0 \exp(Q/k_B T) \quad (13)$$

where v^* is the critical volume at which atomic diffusive process can occur freely [41]. It yields the temperature dependence of internal friction

$$F^{-1}(\beta, T) = F_0^{-1} e^{-\beta} e^{\beta T/T_0} \quad (14)$$

where $\beta(= \gamma v^*/v_f)$ is the free volume parameter which can be obtained independently from thermal expansion and viscosity measurements [42]. $T_0 \simeq T_g$ and physically reasonable coupling constant $F_0^{-1} \simeq 0.3$. The model also predicts the endothermic specific heat of annealed samples and reversible changes in many properties with temperature cycling [39].

The above-mentioned free volume model deals with simple atomic interacting systems and gives a single broad distribution of relaxation times (or glass transitions). In many ternary and quaternary amorphous alloys, there exist two types of short-range ordering, e.g. metal–metal and metal–metalloid types, and the latter shows much stronger ordering than the former. This is manifested by a drastic increase in T_g with the addition of metalloid elements in metal–metalloid amorphous alloys. We thus expect higher mobility or faster relaxation for the metal–metal than for the metal–metalloid pairs.

Taking account of two types of atomic pairs existing in the Fe–Ni–P and Fe–Ni–B amorphous alloys, we propose the existence of two distributions of glass transitions centring at T_{g1} and T_{g2} respectively (see Fig. 25). T_{g1} corresponds to glass transition arising from the metal atoms and T_{g2} to that from metal–metalloid atoms. The relaxation spectra are seen to be asymmetrical with a long tail in the short time. The metal–metal pairs are more or less confined in the skeleton of metal–metalloid pairs. The local range rearrangement of metal atoms with a weak bonding occurs in the low temperature range near T_{g1}, while the atomic regroupings involving metal–metalloid atoms take place at higher temperatures near T_{g2}. This new viewpoint is substantiated from the results [43] that the low temperature endothermic peak is barely detectable in the binary alloys such as Fe–P, Ni–P, Fe–B and Ni–B and the alloying of metallic components leads to an increase in $\Delta C_{p,endo}$ values as well as $\Delta C_{p,exo}$ at the first stage.

The occurrence of the minimum phenomenon in the $\Delta C_{p,r,endo}$ and $\Delta H_{r,endo}$ spectra shown in Figs. 4, 12, 13, 15, and 16 can be explained by taking into consideration of the two distributions of glass transitions. As illustrated in Fig. 25, at $T_a = T_{g2}$, the

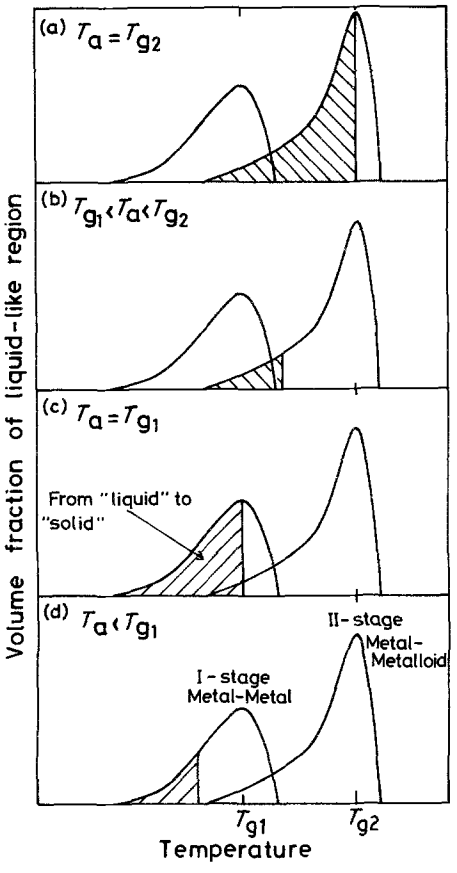

Figure 25 A schematic illustration showing the two-stage distribution of the volume fraction of "liquid"-like unrelaxed region as a function of temperature for a metal–metal–metalloid amorphous alloy.

nearly whole spectrum lies on the shorter side of annealing time ($\tau_m < t_a$), so that almost all the "liquid"-like region undergoes the transition to "solid"-like structure, namely structural relaxation. Similarly, as T_a lowers, the fraction of the change from "liquid"-like region to "solid"-like region on annealing, which is presented by the oblique lines in Fig. 25, decreases, resulting in a reduction of $\Delta C_{p,r,endo}$ and $\Delta H_{r,endo}$. The detectable amount of $\Delta C_{p,r,endo}$ and $\Delta H_{r,endo}$ with DSC at $T_{g1} < T_a < T_{g2}$ is limited to the small region represented with oblique lines and does not include the first-stage relaxation by metal (iron and nickel) atoms, since at $T_a > T_{g1}$ the amorphous region with glass transition of T_{g1} is in the supercooled liquid and hence no transition from "liquid" to "solid" occurs. This is thought to be the reason why the minimum phenomenon appeared in the $\Delta C_{p,endo} - T_a$ and $\Delta H_{r,endo} - T_a$ relations.

4.4. Correlation between two-stage enthalpy relaxation and Curie temperature

It was described in Section 3.5 that the change in T_c of $(Fe_{0.5}Ni_{0.5})_{83}P_{17}$ amorphous alloy with T_a and t_a can be divided to three types: (1) an irreversible rise of T_c from 465 to 480 K at $T_a \leqslant 400$ K; (2) a reversible rise of T_c from 480 K to $T_{c,a}$ at $400 \leqslant T_a \leqslant 500$ K; and (3) a reversible lowering of T_c from 480 K to $T_{c,a}$ at $550 \leqslant T_a \leqslant T_g$. The irreversible rise of T_c corresponds to the irreversible structural relaxation accompanied with exothermic amount $\Delta H_{i,exo}$ shown in Figs. 1 and 3 and has been interpreted as due to the increase in the atomic packing arising from the annihilation of various kinds of quenched-in "defects"such as vacancies, voids, density fluctuations and concentration fluctuations and the enhancement of topological and chemical short-range orderings. The remarkable feature in the data presented in Fig. 19 is that the reversible change of T_c can be distinguished at two stages. Furthermore, each T_a range where the reversible rise and lowering of T_c are observed agrees almost completely with those of the first-stage and the second-stage peaks, respectively, of $\Delta C_p - T_a$ and $\Delta H_{r,endo} - T_a$ curves. The noteworthy result indicates that for the two-stage endothermic reaction, the low-temperature one results in a structural relaxation and a rise of T_c while the high temperature reaction results in a lowering of T_c. Based on the fact that T_c of Fe–Ni–P amorphous alloys rises with decreasing phosphorus content and with the development of the short-range ordering of iron and nickel atoms, it is suggested that the evolution of the reversible ΔC_p and $\Delta H_{\sigma,endo}$ peaks at the first stage on one hand arises from local and medium range atomic rearrangements among metallic elements leading to the reduction in the average atomic distance between the constituent metal (iron and nickel) atoms and the increase in the average number of metallic atoms at the nearest neighbour position. On the other hand, the high-temperature endothermic reaction at the second stage seems to originate from the cooperative rearrangement among metal and metalloid atoms leading to a decrease in average atomic distance between metal and metalloid elements and an increase in average number of metalloid atoms at the nearest neighbour site, resulting in a reduction in T_c.

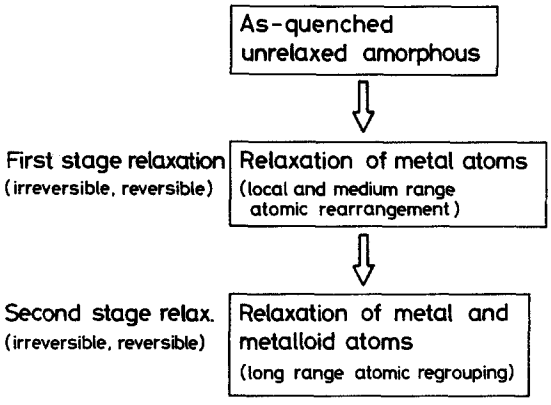

Figure 26 Irreversible and reversible structural relaxation processes of a metal–metal–metalloid amorphous alloy.

4.5. Possible process of structural relaxation

From the above-described results and discussion, we propose a possible structural relaxation process shown in Fig. 26. The structural relaxation of an amorphous phase is divided into irreversible and reversible processes which consist of two stages; the first stage is the local and medium range rearrangement which occurs by the interaction involving only metal atoms and the second stage is a relatively long-range atomic regrouping which occurs by that between metal and metalloid. The two-stage structural relaxations lead to the annihilation of various kinds of quenched-in "defects" and the enhancement of topological and chemical short-range ordering for the irreversible process and to the enhancement of compositional (chemical) short-range ordering for the reversible process. It is quite encouraging that the newly proposed process can explain many of the phenomenological features observed for low- and high-temperature anneals for a number of amorphous alloys such as Fe–Ni–Si–B [5], Fe–Ni–P, Fe–Ni–B, Fe–B [43], Fe–P [43], Ni–P [43], Fe–Co–Si–B [5], Fe–Si–B [5], Co–Si–B [5], and Pd–Ni–Si [44]. Since the relaxation due to the interaction of metal–metal atoms can be faster by a factor of many orders of magnitude than the cooperative relaxation process due to metal–metalloid atoms responsible for the commonly observed glass transition, the concept of the distribution of the glass transition due to metal–metal atoms with short relaxation time is significant and is valuable for an understanding of the stability of amorphous alloys at low temperatures.

4.6. Comparison of $C_p(T)$, $\Delta C_{p,i,exo}$ and $\Delta H_{i,exo}$ between Fe–Ni–P and Fe–Ni–B alloys

The data on the $C_p(T)$, $\Delta C_{p,exo}(T)$ and $\Delta H_{i,exo}$ presented in Section 3 indicate the existence of significant differences in these thermodynamic parameters between Fe–Ni–P and Fe–Ni–B alloys. They may be summarized as follows: (1) while the C_p values near room temperature are nearly equal with each other, the values in the temperature range above about 575 K as well as the temperature dependence of the C_p values are larger for the Fe–Ni–B than for the Fe–Ni–P; (2) the reversible endothermic peaks $\Delta C_{p,r,endo}$, and the irreversible exothermic relaxation occur at two stages, but the temperatures of each peak are higher by about 85 to 110 K for the Fe–Ni–B alloy; (3) the $\Delta H_{i,exo}$ is larger by a factor of about 1.5 for the Fe–Ni–P than for the Fe–Ni–B. From these differences, it is said that the Fe–Ni–B alloy has a high resistance against the irreversible structure relaxation, in particular at lower temperatures. Although the reason for the high thermal stability for the Fe–Ni–B alloy against the structural relaxation remains unknown within the present work, it may be due to the difference in the bonding force between metals (iron and nickel)–metalloids (phosphorus and boron). Considering the result that the Vickers hardness of the amorphous alloys is about 515 DPN for $(Fe_{0.5}Ni_{0.5})_{83}P_{17}$ and about 565 DPN for $(Fe_{0.5}Ni_{0.5})_{83}B_{17}$, the bonding force between metal and meatlloid atoms is considerably larger for metal–boron than for metal–phosphorus. The stronger bonding nature causes a reduction of the atomic mobilibity, resulting in a suppression of structural relaxation. Additionally, the large values of $C_{p,s}$ as well as the temperature coefficient of $C_{p,v}$ for the Fe–Ni–B alloy imply that the free energy at temperatures above about 575 K is lower for the Fe–Ni–B alloy. This suggests that the amorphous structure in Fe–Ni–B system is also more stable from thermodynamic point of view. Anyhow, the higher thermal stability for the Fe–Ni–B alloy may be concluded to originate from the stronger bonding nature of iron or nickel and boron as compared with that of iron or nickel and phosphorus.

5. Conclusion

In order to obtain a further detailed information on the two-stage enthalpy relaxation, which was

previously found for (Fe, Co, Ni)$_{75}$Si$_{10}$B$_{15}$ amorphous alloys for the first time, and to clarify the mechanism for the splitting to the two stages, structural relaxation behaviour of $(Fe_{0.5}Ni_{0.5})_{83}P_{17}$ and $(Fe_{0.5}Ni_{0.5})_{83}B_{17}$ amorphous alloys was investigated calorimetrically for the pre-annealed samples over a wide temperature range from well below to the glass transition temperature, T_g. The results obtained are summarized below.

1. Upon heating the annealed samples, an excess endothermic reaction (enthalpy relaxation) occurs above the annealing temperature T_a and is followed by a broad exothermic reaction. The endothermic specific heat $\Delta C_{p,endo}$, the magnitude of the enthalpy relaxation $\Delta H_{\sigma,endo}$ and the peak temperature of the endothermic reaction T_m increase in a continuous manner with logarithm of t_a, ln t_a.

2. The changes in the magnitude of the $\Delta C_{p,r,endo}$, peak and the $\Delta H_{\sigma,endo}$ with T_a can be distinguished at two stages; a low-temperature (first-stage) peak at about $T_g - 200$ K and a high-temperature (second-stage) peak at a temperature slightly below T_g. The activation energy increases with increasing T_m from 1.7 eV at $T_m = 475$ K to 2.5 eV at $T_m = 600$ K for the Fe–Ni–P and from 1.8 eV at 560 K to 2.0 eV at 620 K for the Fe–Ni–B for the first-stage ($T_a < T_g - 120$ K) relaxation and from 2.6 eV at 600 K to 5.0 eV at 650 K for the Fe–Ni–P for the second-stage ($T_g - 120$ K $< T_a < T_g$) relaxation.

3. The T_a dependence of the Curie temperature T_c of $(Fe_{0.5}Ni_{0.5})_{83}P_{17}$ alloy pre-annealed at 640 K for 1 min can be also separated into two stages; a low temperature region (400 to 550 K) where T_c rises reversibly, and a high temperature region (550 to 625 K) where T_c lowers reversibly.

4. From the almost complete agreement of the temperature range and the peak temperature for the two stages of $\Delta C_{p,r,endo}$, $\Delta H_{\sigma,endo}$ and T_c as well as the marked contrast of the rise and lowering of T_c, the endothermic reaction may be concluded to be due to the local and medium range rearrangements of metal atoms so as to raise T_c for the first-stage peak and to the long-range cooperative rearrangements of metal and metalloid atoms so as to reduce T_c for the second-stage peak, by which each region recovers from relaxed configuration caused by annealing to unrelaxed initial structure.

5. The interpretation of the occurrence of the two-stage reversible enthalpy relaxation as a function of T_a was given within the new concept of two distribution of glass transitions centring at T_{g1} and T_{g2} which arise respectively from metal atoms and from metal–metalloid atoms.

6. In order to interpret reasonably the results obtained in the present work, a possible structural relaxation mechanism leading to the annihilation of various kinds of frozen-in "defects" and the development of topological and compositional short-range ordering was proposed; as-quenched unrelaxed amorphous → irreversible and reversible relaxation of metal atoms in local and medium range → irreversible and reversible relaxation of metal and metalloid atoms over a long range. The newly proposed structural relaxation mechanism is believed to give fairly well an explanation on many of the phonomenological features in the structural relaxation observed for the anneals in the whole temperature below T_g.

References

1. F. E. LUBORSKY, (ed.) "Amorphous Metallic Alloys" (Butterworths, London, 1983).
2. H. S. CHEN, *J. Appl. Phys.* **52** (1981) 1868.
3. *Idem*, Proceedings of the 4th International Conference on Rapidly Quenched Metals, edited by T. Masumoto and K. Suzuki (Japan Institute of Metals, Sendai, 1982) p. 495.
4. J. W. DRIJVER, A. L. MULDER and S. RADELAAR, *ibid.*, p. 535.
5. A. INOUE, T. MASUMOTO and H. S. CHEN, *J. Mater. Sci.* **19** (1984) 3953.
6. H. S. CHEN, *J. Non-Cryst. Solids* **46** (1981) 289.
7. H. S. CHEN and E. COLEMAN, *Appl. Phys. Lett.* **28** (1976) 245.
8. A. J. DAVACS, *Fotchr. Hochpolym-Forsch* **3** (1963) 394.
9. H. S. CHEN, *J. Appl. Phys.* **49** (1978) 4595.
10. R. O. SUZUKI and P. H. SHINGU, *J. Non-Cryst. Solids* **61/62** (1984) 1003.
11. H. S. CHEN, H. J. LEAMY and M. BARMATZ, *ibid.* **5** (1971) 448.
12. M. BARMATZ and H. S. CHEN, *Phys. Rev.* **139** (1974) 4073.
13. B. S. BERRY and W. C. PRITCHER, *J. Appl. Phys.* **44** (1973) 3122.
14. T. SOSHIRODA, M. KOIWA and T. MASUMOTO, *J. Non-Cryst. Solids* **21** (1976) 688.
15. H. S. CHEN, R. C. SHERWOOD, H. J. LEAMY and E. M. GYORGY, *IEEE Trans. Mag.* **MAG-12** (1976) 933.
16. T. EGAMI, *Mater. Res. Bull.* **13** (1978) 557.
17. H. S. CHEN, *J. Appl. Phys.* **49** (1978) 4595.
18. A. L. GREER and J. A. LEAKE, *J. Non-Cryst. Solids* **38-39** (1980) 379.
19. H. S. CHEN, *J. Appl. Phys.* **49** (1978) 3289.
20. A. KURSUMOVIC, M. G. SCOTT, E. GRIT and R. W. CAHN, *Scripta Metall.* **14** (1980) 1303.

21. B. FOGARASSY, A. BOHONYEI, A. CZIRAKI, I. SZABO, G. Y. FAIGEL, L. GRANASY, T. DEMENY and I. VINCZE, *J. Non-Cryst. Solids* **61/62** (1984) 907.
22. M. BALANZAT, *Scripta Metall.* **14** (1980) 173.
23. M. BALANZAT, C. MAIVY and J. HILLARET, *J Phys.* **C-8** (1980) 871.
24. J. HILLAIRET, E. BALANZAT, N-E. DERRADJI and A. CHAMBEROD, *J. Non-Cryst. Solids* **61/62** (1984) 781.
25. A. J. DREHMAN and W. L. JOHNSON, *Phys. Status Solidi (a)* **52** (1979) 499.
26. A. RAVEX, J. C. LASJAUNIAS and O. BETHOUX, *Physica* **107B** (1981) 397.
27. C. C. KOCH, D. M. KROEGER, J. S. LIN, J. O. SCARBROUGH, W. L. JOHNSON and A. C. ANDERSON, *Phys. Rev.* **27** (1983) 1586.
28. A. INOUE, S. OKAMOTO, N. TOYOTA, T. FUKASE, K. MATSUZAKI and T. MASUMOTO, *J. Mater. Sci.* **19** (1984) 2719.
29. A. INOUE, K. MATSUZAKI, N. TOYOTA, H. S. CHEN, T. MASUMOTO and T. FUKASE, *ibid.* in press.
30. H. S. CHEN, *Mater. Sci. Eng.* **26** (1976) 79.
31. A. INOUE, H. M. KIMURA and T. MASUMOTO, *J. Jpn. Inst. Metals* **42** (1978) 303; *Rep. Res. Int. Tohoku Univ.* **A-27** (1979) 159.
32. H. S. CHEN, *J. Non-Cryst. Solids* **27** (1978) 257.
33. T. OZAWA, *Polymer* **12** (1971) 51.
34. C. ANTONIONE, L. BATTEZZATI, A. LUCCI, G. RIONTINO and G. VENTURELLO, *Scripta Metall.* **12** (1978) 1011.
35. H. S. CHEN, *Sci. Rep. Res. Inst. Tohoku Univ.* **A-27** (1979) 97.
36. W. PRIMAK, *Phys. Rev.* **100** (1955) 1677.
37. M. H. COHEN and G. S. CREST, *ibid.* **B20** (1979) 1077.
38. M. CYAT, *J. Phys.* **C-8** (1980) 107.
39. H. S. CHEN and N. MORITO, manuscript in preparation.
40. H. S. CHEN and N. MORITO, "Rapidly Quenched Metals 5" Würzburg, Federal Republic of Germany 3-7 September (1984) in press.
41. M. H. COHEN and D. TURNBULL, *J. Chem. Phys.* **31** (1959) 1164.
42. H. S. CHEN, *J. Non-Cryst. Solids* **29** (1978) 223.
43. A. INOUE, T. MASUMOTO and H. S. CHEN, unpublished research (1984).
44. H. S. CHEN and A. INOUE, *J. Non-Cryst. Solids* **61/62** (1984) 805.

Received 23 July
and accepted 31 July 1984